Assessment of Corrosive Attack of Fe9Cr1Mo alloys in Pressurised CO_2 for Prediction of Breakaway Oxidation

Supplementary Materials: Review of DiCTra Simulations and Comparisons with Numerical Models Developed by Gong *et al.*

Henrik Larsson

Thermo-Calc Software, Råsundavägen 18, SE-16967 Solna, Sweden
Department of Materials Science and Engineering, KTH Royal Institute of Technology, SE-100 44 Stockholm, Sweden

1 Background

The purpose of the present work is to review the DiCTra [1] simulations performed in the work by Gong and Reed [2]. Work closely related to Ref. [2] is described in the article by Gong et al. [3].

The structure of this report is as follows. In section 2 the DiCTra homogenization model is described with special emphasis on details relevant for the current work. In section 3 thermodynamic and kinetic data is briefly discussed. In section 4 all specific set-up details for the DiCTra simulations are given. Simulation results are given in section 5 and the final discussion is found in section 6.

2 DiCTra simulation model

In the work by Gong and Reed the so-called DiCTra homogenization model [4][5] was used. Here follow a brief description of the model.

The model is restricted to simulations where concentration is allowed to vary along one spatial coordinate, though the geometry may be planar, cylindrical or spherical.

2.1 Flux in single phase systems

The flux J_k ($\mathrm{mol} \cdot \mathrm{m}^{-2} \cdot \mathrm{s}^{-1}$) of component k along spatial coordinate z is, in the so-called lattice-fixed frame of reference, given by (see, e.g. Refs. [6][7])

$$J_k = -M_k c_k \frac{\partial \mu_k}{\partial z} \quad k = 1, \ldots, n \tag{1}$$

where M_k, c_k and μ_k are the mobility, concentration and chemical potential of component k, respectively. The components are elements in DiCTra. The mobilities are functions of composition and state (phase / temperature / pressure), though the pressure dependency is generally not available. It would be more correct to write the flux expression as $J_k = \sum L_{kj} \partial \mu_j / \partial z$, where the L_{kj} are kinetic coefficients. However, the error introduced by using

the approximate expression Eq. 1 is only about 10% [8][9][10], which is quite small compared to the uncertainties when determining mobilities. The consensus at present is therefore to use Eq. 1 for the flux in the lattice-fixed frame of reference.

The flux J_k in the lattice-fixed frame of reference may be transformed to a flux J'_k in a volume-fixed frame of reference through the relationship

$$J'_k = J_k - c_k v = J_k - c_k \sum V_i J_i \tag{2}$$

where v is the velocity relative to the two frames of references and V_i is the partial molar volume of component i. The assumption traditionally used in DICTRA is that the partial molar volume of interstitial elements is zero and that the partial molar volume of substitutional elements, denoted V_S, is constant and equal [11]. With this assumption, the concentration c_k is given by

$$c_k = \frac{x_k}{V_m} = \frac{u_k}{V_S} \tag{3}$$

where x_k is the mole fraction of element k, V_m is the molar volume and u_k is the so-called u-fraction of element k given by

$$u_k = \frac{x_k}{\sum_{j \in S} x_j} \tag{4}$$

By $j \in S$ should be inferred that the summation is taken over the substitutional elements only. Plotting results as u-fraction profiles can be beneficial since this is a simple way to graphically "decouple" the diffusion of substitutional and interstitial elements.

The flux in the volume-fixed frame of reference is then given by

$$J'_k = J_k - u_k \sum_{j \in S} J_j \tag{5}$$

However, in the work by Gong and Reed a recently implemented feature [12] was used which allow for the use of assessed molar volumes and in which the problem is solved in the lattice-fixed frame of reference. The flux is then only evaluated using Eq. 1.

2.2 Multiphase simulations

The homogenization model is intended for multiphase simulations, i.e. to simulate diffusion through a multiphase mixture taking into account reactions that may occur as a result of the diffusion process; it is a diffusion–reaction simulation model.

As in many other such models (see for example Refs. [13][14]) the basic assumption is that the system is locally equilibrated; the local phase fractions, phase compositions etc. correspond to, a possibly constrained, equilibrium. This is generally an excellent assumption if the diffusion distance considered in the simulation is considerably larger than a characteristic microstructural length scale, such as the interparticle spacing. However, if establishing local equilibrium require substantial diffusion to take place inside, for example, carbide phases the assumption may not apply, see for example Ref. [15]. Another case for which the model must be used with caution is when rapid temperature variations occur.

In order to estimate the effective kinetic properties of a multiphase mixture it is convenient to introduce the permeability, which for phase r is given by

$$\Gamma_k^r = M_k^r c_k^r \tag{6}$$

The effective permeability of the multiphase mixture is denoted $\Gamma_k^\star$ and must be estimated by some suitable assumption as discussed below in section 2.3. The flux through the multiphase mixture is then obtained by slightly rewriting Eq. 1 as

$$J_k = -\Gamma_k^\star \frac{\partial \mu_k^{\text{l.eq.}}}{\partial z} \tag{7}$$

where the superscript *l.eq.* has been added to emphasize that local equilibrium is assumed to hold.

2.3 Homogenization function — evaluation of $\Gamma_k^\star$

There are a number of different possibilities to estimate the effective permeability $\Gamma_k^\star$ of a multiphase mixture, but there are essentially only two approaches that can be justified theoretically, viz. the Wiener bounds [16] (rule of mixtures) and the Hashin–Shtrikman bounds [17]. The Wiener bounds are given by

$$\Gamma_k^\star = \sum_r f^r \Gamma_k^r \tag{8}$$

$$\Gamma_k^\star = \left[\sum_r \frac{f^r}{\Gamma_k^r} \right]^{-1} \tag{9}$$

for the upper and lower bound, respectively. f^r is the volume fraction of phase r. Geometrically, the Wiener bounds correspond to continuous layers of the phases present either parallel with (upper bound) or orthogonal to (lower bound) the direction of diffusion.

Hashin and Shtrikman used a variational approach to derive their bounds assuming that the multiphase material is macroscopically homogeneous and isotropic. Their bounds are given by

$$\begin{aligned} \Gamma_k^\star &= \Gamma_k^s + \frac{A_k^s}{1 - \dfrac{A_k^s}{3\Gamma_k^s}} \\ A_k^s &= \sum_{r \neq s} \frac{f^r}{\dfrac{1}{\Gamma_k^r - \Gamma_k^s} + \dfrac{1}{3\Gamma_k^s}} \end{aligned} \tag{10}$$

where, if m different phases are considered,

$$\Gamma_k^s = \min\{\Gamma_k^1, \ldots, \Gamma_k^m\} \tag{11}$$

$$\Gamma_k^s = \max\{\Gamma_k^1, \ldots, \Gamma_k^m\} \tag{12}$$

for the lower and upper bound, respectively. For the case of a two-phase mixture where the permeability is zero in one of the phases, the upper bound is identical to the leading term in the formula derived by Rayleigh [18] for spherical diffusion-blocking precipitates set on a cubic lattice.

A so-called labyrinth function [14] is sometimes used ad hoc when diffusion is assumed to occur in a single matrix phase only, as in the present case. It is simply given by

$$\Gamma_k^\star = (f^s)^n \, \Gamma_k^s \tag{13}$$

where s is the matrix phase. The exponent n is typically in the range of 1–3.

The default homogenization function is the upper Wiener bound, which is identical to the labyrinth function with $n = 1$ when diffusion occurs in a single matrix phase only. For moderate volume fractions of zero diffusivity phases, it seems to be a reasonable choice, see e.g. Ref. [19] where coupled carbonitriding and internal oxidation was simulated for steel containing 1.15Cr-0.95Mn-0.27Si and a good agreement with experimental data was obtained. On the other hand, in Ref. [14] carburisation of a Ni-25Cr alloy was simulated and a labyrinth function with exponent $n = 3$ was needed to obtain a reasonable agreement with experimental data obtained from Ref. [20], but the carbide phases then almost cover all grain boundaries. The choice of homogenization function can thus be quite difficult and some knowledge of the distribution and morphology of phases is very useful for the selection process.

In the present case, both the upper Wiener bound and the upper Hashin–Shtrikman bound are reasonable choices.

2.4 Conservation law

The expression for the flux is combined with the equation of continuity, which for a planar geometry is given by

$$\frac{\partial c_k}{\partial t} = \frac{\partial}{\partial z} \left(-J_k \right) \quad k = 1, \ldots, n \tag{14}$$

The set of non-linear partial differential equations (PDEs), Eqs. 7 and 14, together with a given initial state and boundary conditions (BCs), are solved to yield the temporal evolution of the concentration fields. Since the problem is solved using assessed molar volumes the size of the domain will generally change during the diffusion process.

The flux of vacancies is not explicitly treated; it is assumed that vacancies are created and annihilated such that an equilibrium amount is maintained. The flux of vacancies in a specific phase on a given sublattice may, however, be calculated under the assumption that it is equal to minus the sum of all diffusing constituents on that sublattice. Such calculations may then be used to estimate the amount of Kirkendall porosity [21][22].

2.5 Temperature and pressure

Any pressure dependencies are generally ignored and a default pressure of 1 bar is assumed throughout the domain.

Even if the temperature is allowed to vary spatially it is normally assumed that the temperature is the same throughout the domain; DICTRA has no capability to solve for any spatial variation in temperature due to reactions occurring. Temperature as a function of time may be input in a quite general manner with an arbitrary number of piece-wise functions, though there should be no discontinuities.

2.6 Boundary conditions

Many different types of boundary conditions have been implemented. Besides a closed system, fluxes or activities (chemical potentials) may for example be prescribed on the boundary. Boundary conditions may in most cases be entered as functions of time and temperature. Different types of boundary conditions may also, to some extent, be mixed such that different conditions apply to different components. The size of the domain may be allowed to change as a result of the boundary conditions.

The boundary condition used by Gong and Reed, is a so-called activity flux function [23]. This BC is the best choice for the current work. The flux across the boundary is then given by

$$J_k = f_k \left(a_k^N - g_k \right) \tag{15}$$

where f_k, g_k and N is input from the user. The activity a_k is evaluated from the composition of the finite volume at the boundary.

It should be noted that when the problem is solved in the DICTRA volume-fixed frame of reference, the evaluated quantity from the input functions f_k, g_k and N is $J_k \cdot V_S$. When the problem is solved in the lattice-fixed frame of reference using the assessed molar volumes from the thermodynamic database the flux at the boundary is as given by Eq. 15. Thus, the unit of f_k differs depending on whether the problem is solved in the DICTRA volume-fixed frame of reference or the lattice-fixed frame of reference.

2.7 Numerical implementation

The model has been implemented as a finite volume method (FVM) with implicit (Euler backward) or semi-implicit (trapezoidal rule) time-stepping. Time-step control is automatic and the choice of time-step is obtained by inspecting the truncation error found by Richardson extrapolation.

Schematically, the non-linear, multivariable problem to solve each time-step Δt is

$$\mathbf{F} = \hat{\mathbf{c}} \left(\mathbf{c} \left(t + \Delta t \right) \right) - \mathbf{c} \left(t + \Delta t \right) = \mathbf{0} \tag{16}$$

where $\mathbf{c}$ is a vector containing the, initially unknown, compositions of all components at all grid points at the end of the time step. $\hat{\mathbf{c}}$ is likewise a vector containing the compositions of all components at all grid points at the end of the time-step, but evaluated from $\mathbf{c}$, the state at the beginning of the time-step and the boundary conditions. In order to solve for $\mathbf{c}$, Eq. 16 is expanded using an initial guess of $\mathbf{c}$

$$\mathbf{F} \simeq \mathbf{F_0} + \mathbb{J} \Delta \mathbf{c} = 0 \tag{17}$$

and Eq. 17 is then solved iteratively for $\Delta \mathbf{c}$ whereupon $\mathbf{c} \rightarrow \mathbf{c} + \Delta \mathbf{c}$ until $|\mathbf{F}| < \varepsilon$ for all F. The Jacobian matrix $\mathbb{J}$ is evaluated by numerical perturbations; analytical partial derivatives are not available.

The discretisation (grid point distribution) can be chosen quite arbitrarily, but there should not be any large and abrupt changes in the grid point distribution. Grid point positions can be entered manually or read from a file, but commonly equidistant ("linear") grids, geometrical grids or a combination thereof are used. For a geometrical grid, the distance between neighbouring grid points is consecutively changed by a given factor. This factor will normally be in the range of 0.9–1.1.

The only reasonable choice for the simulations in the present work is a geometrical grid.

Further general reading can be found in, for example, the textbooks by Dahlqvist and Björk [24] and Nocedahl and Wright [25].

3 Thermodynamic and kinetic data

The thermodynamic and kinetic databases supplied by Thermo-Calc software are well assessed. However, it is an inherent shortcoming of the CalPhaD method [26] that it is very difficult to estimate uncertainties. For critical simulations, it is good practice to check the original references as well as database descriptions.

The system under consideration in the present work, FeCrMoC, is of fundamental importance to the steel industry and the underlying thermodynamic assessments are therefore very well scrutinized and there is a wealth of experimental data that was used in the assessment work. The entire quaternary system was assessed by Qiu [27]. A slight modification of Qiu's assessment was made by Bratberg [28].

For the current work, the only kinetic data of interest is essentially the carbon diffusion in ferrite (α). The mobility of carbon in ferrite was assessed by Jönsson [29]. He obtained very good agreement with experimental data from multiple sources over a wide temperature range.

The compositions under consideration are well below the recommended maximum limits of TCFE8 for C, Cr and Mo [30].

The choice of phases to include in simulations must also be considered. In the present case the diffusion of Fe, Cr and Mo is essentially insignificant compared to that of C and a plot of phase fractions as a function of carbon activity at relevant temperatures can be used as an initial screening. As per instructions the current simulations were mainly run with α, $M_{23}C_6$, M_7C_3 and M_6C. A plot of phase fractions as a function of carbon activity shows that also M_3C_2 is stable at 400°C for carbon activities above 0.23. At 640°C cementite is stable for carbon activities above 0.93.

4 Summary of simulation set-up used in present work

All simulations in the current work were performed with the most recent version of Thermo-Calc, version 2019a, except that it turned out that an error had been introduced between versions 2018b and 2019a; this error ("bug") was removed in the version used to run simulations; the bug-fix will be included in Thermo-Calc 2019b.

The thermodynamic database TCFE8 and the kinetic database MOBFE4 were used. Phases participating in the simulation were in one set of simulations BCC (ferrite, α), $M_{23}C_6$, M_7C_3 and M_6C. In another set of simulations only α and $M_{23}C_6$ participated. The thermodynamic description of graphite is also read from TCFE8 since the reference state of carbon was set as graphite at ambient temperature and pressure. For all these phases, kinetic data is only available for the ferrite. The mobilities in the carbides are therefore implicitly set to zero, which is an excellent approximation since diffusion is very sluggish in the carbides compared to the ferrite.

Unless otherwise explicitly stated, the following settings were used in DiCTra:

- An initial domain size of 500 μm with a planar geometry
- A geometrical type of grid with 80 points and a coefficient of 1.07
- Fully implicit time-stepping (Euler backward)
- The upper Wiener bound (rule of mixtures) was used as homogenization function
- The material was assumed to be initially homogeneous with the composition 9Cr, 1Mo, 0.1C (bal. Fe, mass-%)

	α_a							
T [°C]	c1	c2	c3	c4	c5	c6	c7	c8
400	1.01E-11	4.28E-12	1.80E-12	7.61E-13	3.21E-13	1.36E-13	5.72E-14	2.41E-14
450	2.43E-10	1.14E-10	5.38E-11	2.53E-11	1.19E-11	5.59E-12	2.63E-12	1.24E-12
485	1.75E-09	8.81E-10	4.43E-10	2.23E-10	1.12E-10	5.64E-11	2.84E-11	1.43E-11
520	1.06E-08	5.67E-09	3.03E-09	1.62E-09	8.67E-10	4.64E-10	2.48E-10	1.33E-10
550	4.39E-08	2.47E-08	1.38E-08	7.77E-09	4.36E-09	2.45E-09	1.37E-09	7.71E-10
580	1.65E-07	9.67E-08	5.68E-08	3.34E-08	1.96E-08	1.15E-08	6.75E-09	3.96E-09
600	3.78E-07	2.28E-07	1.38E-07	8.33E-08	5.03E-08	3.04E-08	1.84E-08	1.11E-08
620	8.36E-07	5.19E-07	3.22E-07	2.00E-07	1.24E-07	7.69E-08	4.77E-08	2.96E-08
640	1.78E-06	1.14E-06	7.24E-07	4.61E-07	2.94E-07	1.87E-07	1.19E-07	7.58E-08

Table 1: Interface reaction parameter values used in simulations. From Gong and Reed [2].

- The problem was solved in the lattice-fixed frame of reference using the assessed molar volumes
- The input parameters N and g_{C} for the lower/left boundary condition, Eq. 15, was set to 1 and 1.0, respectively for carbon. The values used for parameter f_{C} were taken from Gong and Reed, see Table 1. For all other elements, the boundary was closed.
- The upper/right boundary was closed for all elements

Some additional settings motivate brief explanations/motivations:

Plotted (saved) results correspond to the average composition of finite volumes, which is not the default; except for the homogenization model DICTRA is implemented using a finite element method (FEM) in which concentration profiles are piece-wise linear; with FVM it is only the average composition of each finite volume that is known; the default behaviour of the homogenization model is therefore to convert the "FVM-profiles" to "FEM-profiles" such that mass balance is obeyed. The drawback of this conversion is that it may cause oscillations and as a precaution, it was therefore turned off.

At boundaries, the default behaviour is that the flux of the dependent substitutional element (Fe) is evaluated such that the net flow of substitutional elements across the boundary is zero. This default setting was turned off; when solving in the lattice-fixed frame of reference using assessed molar volumes the strict division of elements into substitutionals and interstitials is meaningless and internally all elements are set as substitutional.

By default, a so-called interpolation scheme [31] is used since this usually speeds up simulations. For the simulations in the present work, this was not the case and the interpolation scheme was therefore turned off.

5 Simulation results

5.1 Simulation termination criterion

Gong and Reed defined

$$\eta = \frac{x_{\mathrm{C}} - x_{\mathrm{C}}^{\circ}}{x_{\mathrm{C}}^{\mathrm{eq}} - x_{\mathrm{C}}^{\circ}} \tag{18}$$

as a measure of the Carbon saturation, where x_{C}° is the base carbon content of the alloy and $x_{\mathrm{C}}^{\mathrm{eq}}$ is the equilibrium carbon content corresponding to a Carbon activity $a_{\mathrm{C}} = 1$. They then gave a critical value of η equal to $\eta_{\mathrm{crit}} = 0.8$. This was also used as a termination criterion in the present work. The time to reach this carbon content is denoted t_{crit}. Currently, it is not, however, possible to automatically terminate a simulation based on such a criterion.

It should be noted that the carbon composition "at the boundary" actually corresponds to the average composition of the finite volume at the boundary. An alternative would be to extrapolate using the midpoints of two or three of the finite volumes closest to the boundary, but this could be problematic and is discussed further in section 5.5

	x_C^{eq} (%)			
	$\alpha + M_7C_3$ $+M_{23}C_6 + M_6C$		$\alpha + M_{23}C_6$	
T [°C]	$a_C = 1$	$a_C = 0.8$	$a_C = 1$	$a_C = 0.8$
400	5.605	5.437	4.715	4.553
520	6.769	6.423	6.027	5.649
600	7.864	7.324	7.543	6.832
640	8.507	7.840	8.642	7.642

Table 2: Equilibrium carbon content (mole percent) for Fe9Cr1Mo at $a_C = 1$ and $a_C = 0.8$ for two different sets of phases participating in the equilibrium calculations.

	t_{crit} [kh]		
T [°C]	c1	c4	c8
400	8.39E+04	-	-
520	1.09E+02	6.69E+02	7.61E+03
600	3.69E+00	1.64E+01	1.12E+02
640	8.06E-01	3.31E+00	1.79E+01

Table 3: Time t_{crit} [kh] to reach a carbon content corresponding to $\eta_{crit} = 0.8$ at the surface under different conditions. For these simulations the participating phases were $\alpha + M_7C_3 + M_{23}C_6 + M_6C$. Diffusion of all four elements was included in the simulations, cf. Table 5.

For comparison, the amount of carbon corresponding to $a_C = 1$ and $a_C = 0.8$ for the base alloy composition, i.e. 9 Cr and 1 Mo, are presented in Table 2; the Fe-Cr-Mo atomic ratio was fixed for these calculations.

5.2 Base set of simulations

An initial set of simulations were performed with settings as described in section 4. Results in the form of the critical time t_{crit} to reach $\eta_{crit} = 0.8$ at the surface are given in Table 3. There is essentially perfect agreement with the values obtained by Gong and Reed. The small differences can be due to that the present author chose not to save results from as many time steps as Gong and Reed, or in the method of interpolation; these results were not obtained directly using the DICTRA post processor, but rather by analyzing output from DICTRA.

Some carbon concentration profiles are plotted in Figs. 1–3.

5.3 Effect of reduced number of carbide phases

A second set of simulations were performed that differ from the simulations of section 5.2 in that the only carbide phase that participated was $M_{23}C_6$. Results in the form of the critical time t_{crit} to reach $\eta_{crit} = 0.8$ at the surface are given in Table 4. The time to reach t_{crit} is up to 25% shorter for these simulations compared to the case where all carbide phases participate.

Constraining the equilibrium calculations in this manner should be motivated by experimental observations.

5.4 Effect of diffusion of substitutional elements

A set of simulations were performed where the diffusivities of Cr, Fe and Mo were set to zero. Results in the form of the critical time t_{crit} to reach $\eta_{crit} = 0.8$ at the surface are given in Table 5. Comparing these results with those given in Table 3 it is seen that the effect of diffusion of substitutional elements is relatively small, though increasing with increasing temperature. At this point, it should also be reiterated that the basic assumption

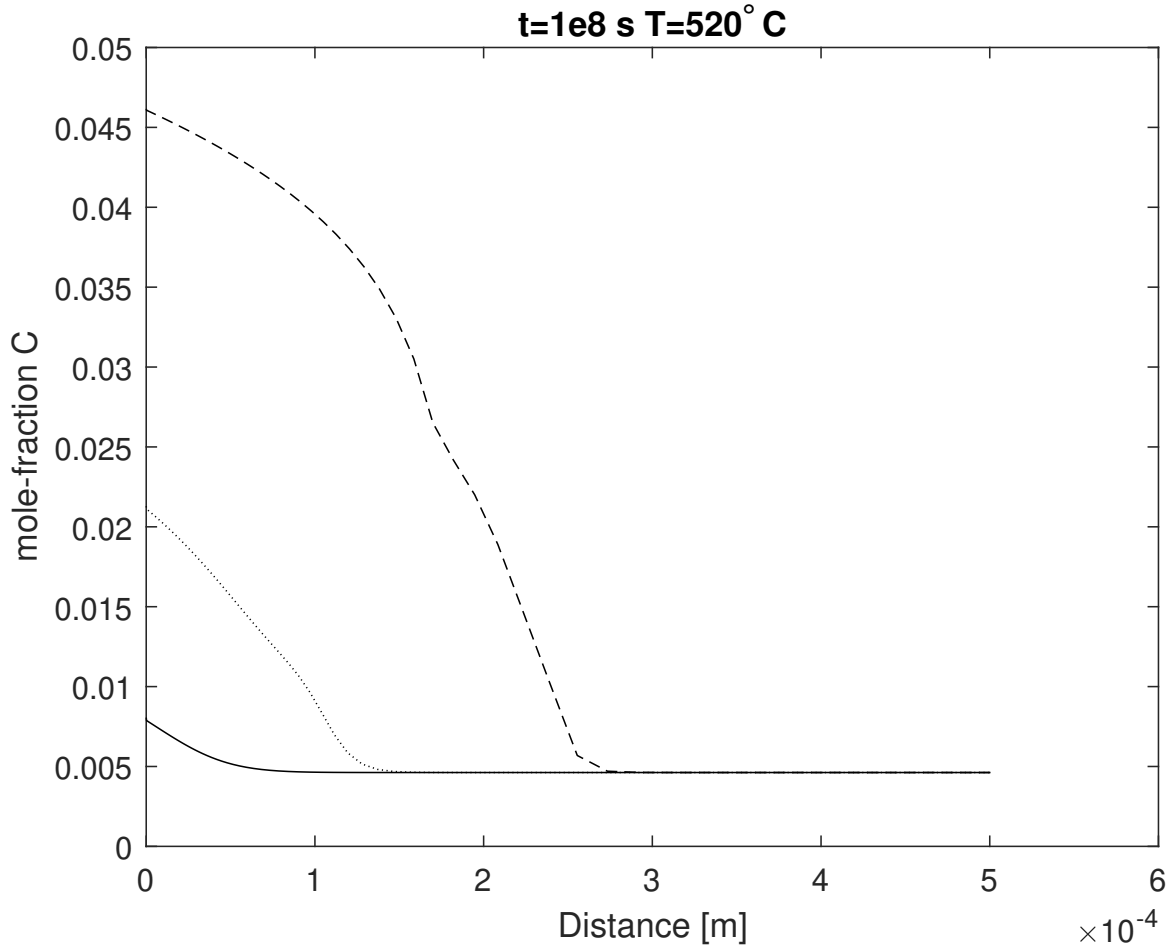

Figure 1: Carbon mole-fraction profiles at T = 520°C and t=1e8 s. The different lines correspond to different interface reaction parameters, viz. column 1 (dashed), 4 (dotted) and 8 (solid) of Table 1. The settings for these simulations are given in section 5.2.

	t_{crit} [kh]		
T [°C]	c1	c4	c8
400	8.39E+04	-	-
520	9.97E+01	6.11E+02	6.78E+03
600	2.83E+00	1.39E+01	9.56E+01
640	6.25E-01	2.92E+00	1.61E+01

Table 4: Time t_{crit} [kh] to reach $\eta_{\text{crit}} = 0.8$ at the surface under different conditions. For these simulations the participating phases were $\alpha + \text{M}_{23}\text{C}_6$. Diffusion of all four elements was included in the simulations.

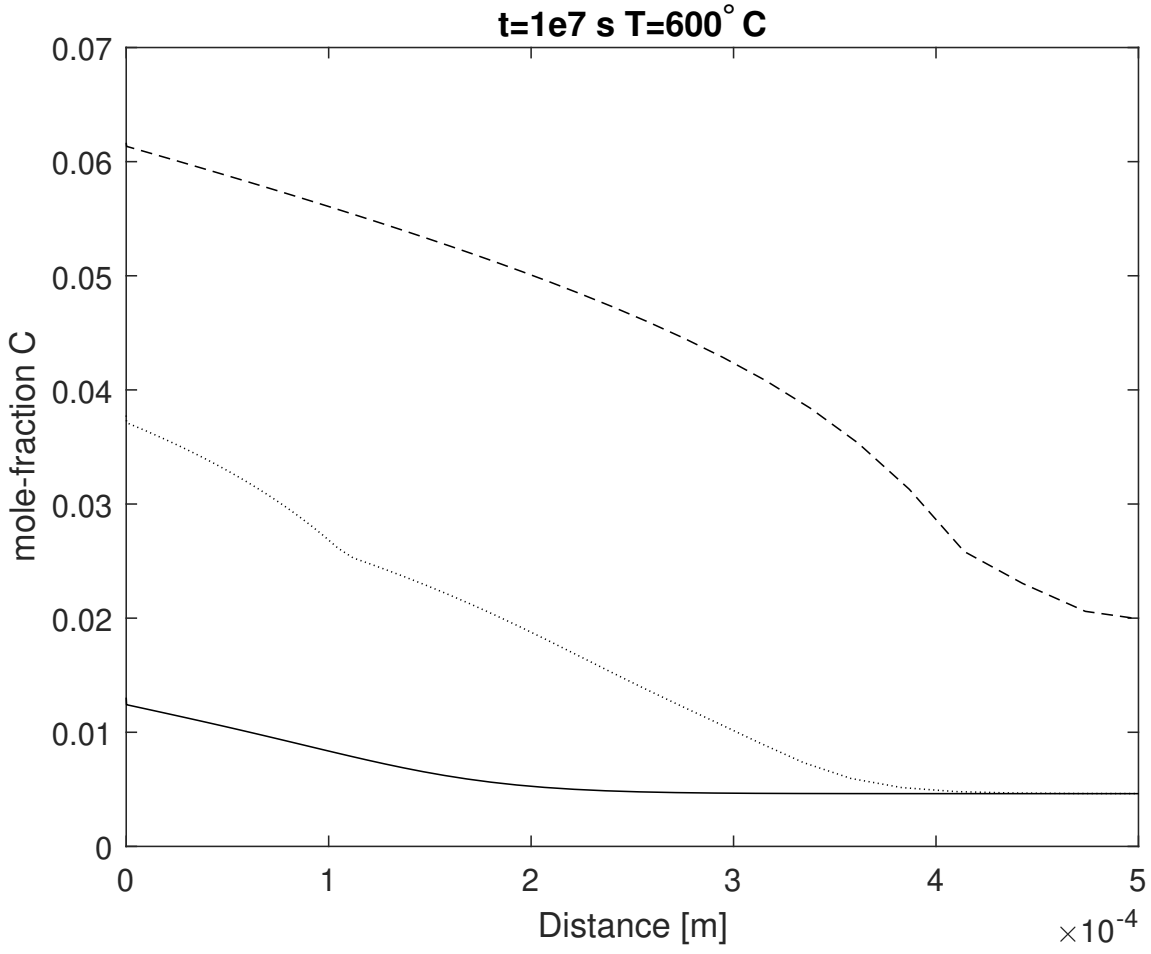

Figure 2: Carbon mole-fraction profiles at T = 600°C and t=1e7 s. The different lines correspond to different interface reaction parameters, viz. column 1 (dashed), 4 (dotted) and 8 (solid) of Table 1. The settings for these simulations are given in section 5.2.

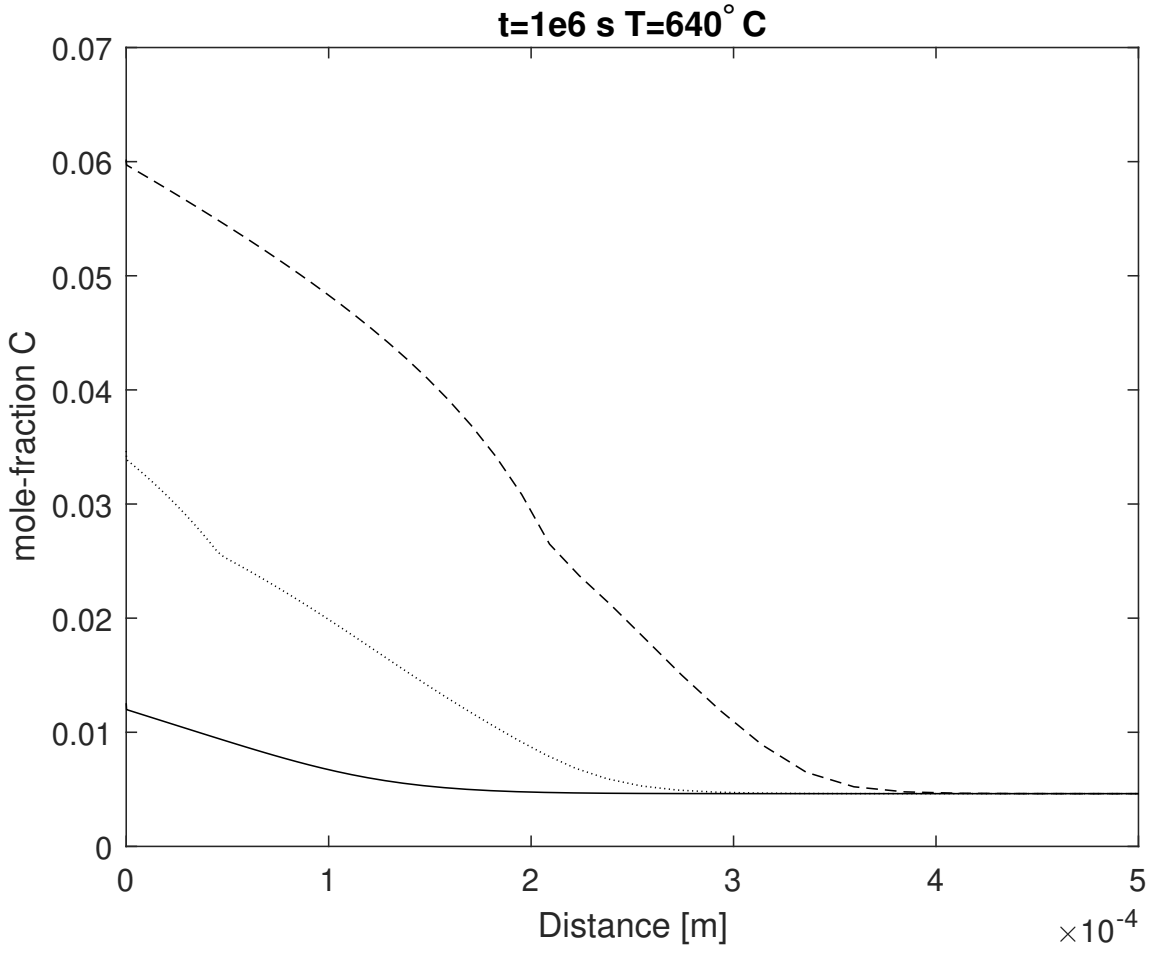

Figure 3: Carbon mole-fraction profiles at T = 640°C and t=1e6 s. The different lines correspond to different interface reaction parameters, viz. column 1 (dashed), 4 (dotted) and 8 (solid) of Table 1. The settings for these simulations are given in section 5.2.

	t_{crit} [kh]		
T [°C]	c1	c4	c8
520	1.09E+02	6.81E+02	-
640	8.64E-01	3.53E+00	2.08E+01

Table 5: Time t_{crit} [kh] to reach $\eta_{\text{crit}} = 0.8$ at the surface under different conditions. For these simulations the participating phases were $\alpha + M_7C_3 + M_{23}C_6 + M_6C$. For these simulations the diffusivities of Cr, Fe and Mo were set to zero, cf. Table 3.

Composition	t_{crit} [kh]
Fe-9Cr-1Mo-0.1C	1.64E+01
Fe-10Cr-1Mo-0.1C	1.49E+01
Fe-8Cr-1Mo-0.1C	1.92E+01
Fe-9Cr-1Mo-0.11C	1.63E+01
Fe-9Cr-1Mo-0.09C	1.65E+01

Table 6: Time t_{crit} [kh] to reach $\eta_{\text{crit}} = 0.8$ at (600°C) for different alloy compositions. For these simulations the participating phases were $\alpha + M_7C_3 + M_{23}C_6 + M_6C$. The interface reaction parameter value used correspond to column c4/600°C in Table 1.

of the simulation model is that equilibrium is reached locally – with respect to those phases that participate in the simulation – which obviously require substitutional diffusion. Separate simulations could be performed to investigate the expected time to locally reach equilibrium, though this would require an estimate of the carbide nucleation density.

5.5 Effect of grid spacing

The effect of different grid point distributions is shown in Figs. 4–7. Three simulations were made where the only difference was the total number of grid points. The simulations were made at 600°C with interface reaction parameter taken from column 4 in Table 1 and participating phases were $\alpha + M_7C_3 + M_{23}C_6 + M_6C$. A geometrical grid with a coefficient of 1.07 with 80, 60 and 40 grid points was used, respectively. The time to reach $\eta_{\text{crit}} = 0.8$ was $t = 16.4, 16.8, 16.9$ [kh], respectively. The notable difference in carbon content close to the surface can clearly be seen in Fig. 5. This is caused by the minute amount of chromium diffusion as can be seen in Fig. 6 where the u-fraction chromium as a function of distance has been plotted; chromium decreases the activity of carbon, which can be seen by comparing Figs. 5–7; the activity profile of carbon is plotted in Fig. 7.

The enrichment of chromium at the surface is thus dependent on the grid spacing. However, as can be seen in Figs. 4–7 the time to reach t_{crit} is virtually not affected. If a thin continuous carbide film could form, similar to oxide formation on stainless steels, the situation would be different, but since this is not the case a suitable grid spacing at the boundary could correspond to the size of the carbides.

5.6 Effect of perturbation in composition

The effect of differences in composition was investigated by running simulations with altered carbon and chromium compositions. Results are listed in Table 6. These results should be compared with the tolerances of the steel manufacturer.

5.7 Effect of ambient carbon activity

The effect of the carbon activity parameter of the boundary condition, i.e. the parameter g_C of Eq. 15, was investigated by comparing results obtained with $g_C = 1.0, 0.95$ and 0.9. Results are listed in Table 7.

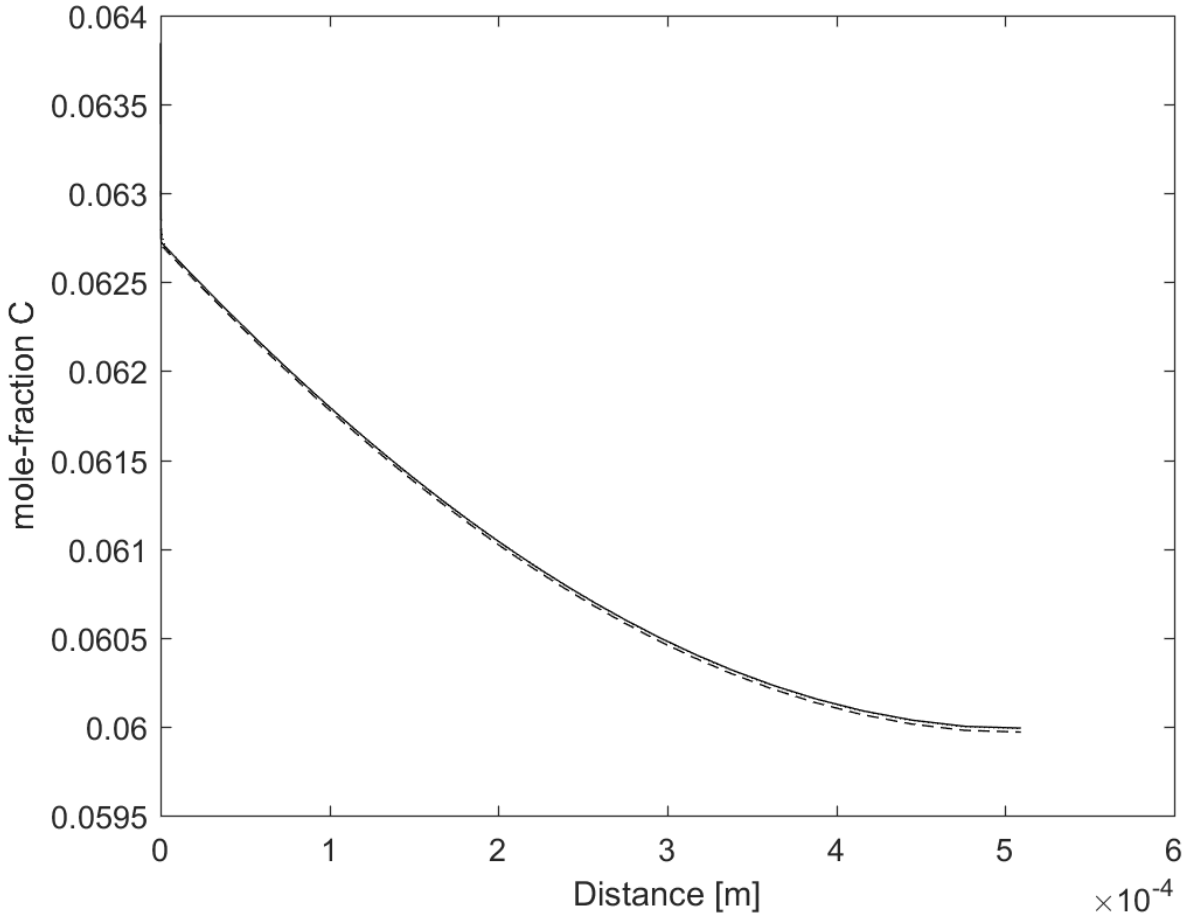

Figure 4: Comparison between results obtained at $t = 5.89 \cdot 10^7$ [s] with different grid point distributions. Mole fraction carbon plotted as a function of distance. Simulations performed at 600°C with interface reaction parameter taken from column 4 in Table 1. Geometrical grid with coefficient 1.07 with 80 (solid line), 60 (dashed line) and 40 (dotted line) grid points, respectively. See also Figs. 5–7.

g_C	t_{crit} [kh]
1.0	1.64E+01
0.95	1.74E+01
0.90	1.86E+01

Table 7: Time t_{crit} [kh] to reach $\eta_{crit} = 0.8$ at (600°C) for different values of g_C. For these simulations the participating phases were $\alpha + M_7C_3 + M_{23}C_6 + M_6C$. The interface reaction parameter value used correspond to column c4/600°C in Table 1.

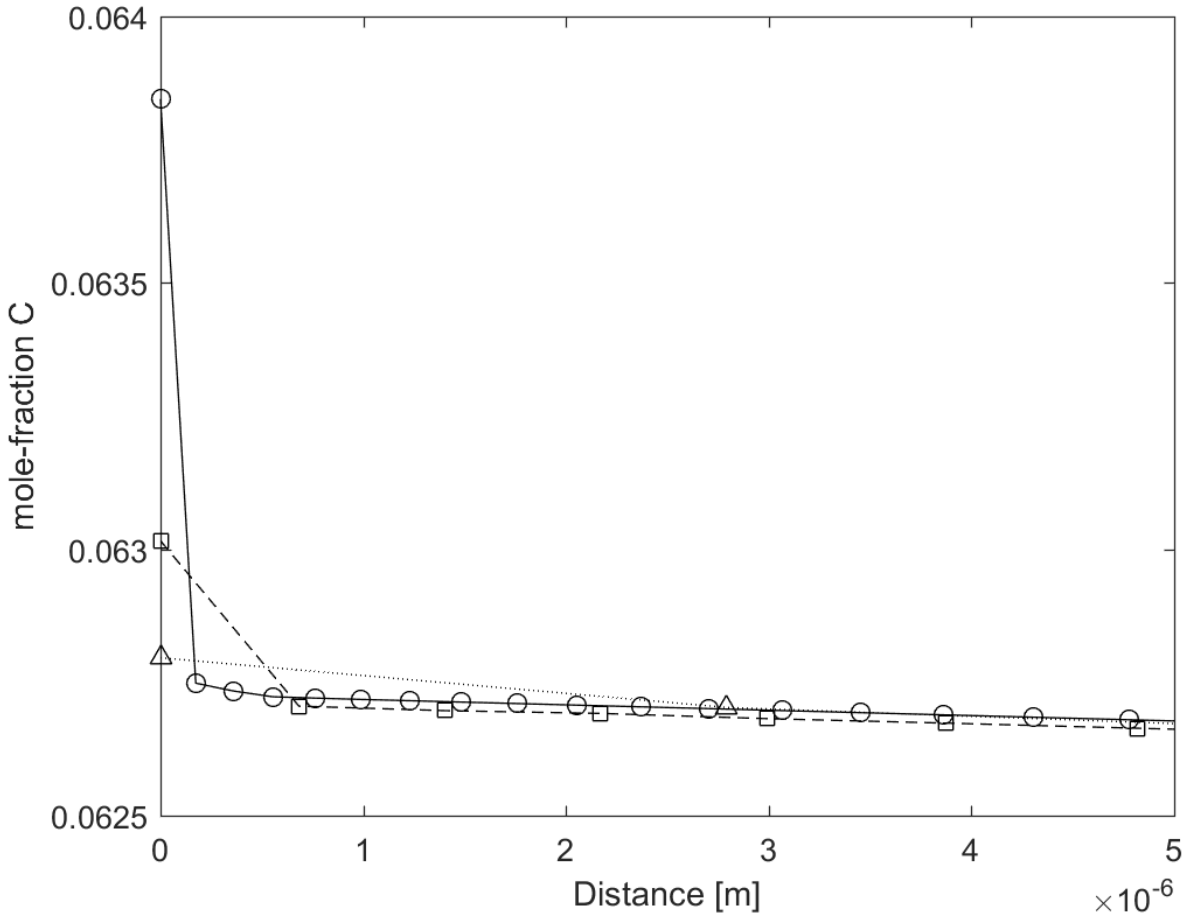

Figure 5: Comparison between results obtained at $t = 5.89 \cdot 10^7$ [s] with different grid point distributions. Mole fraction carbon plotted as a function of distance. Close-up of surface region, cf. Figs. 4, 6, 7. Simulations performed at 600°C with interface reaction parameter taken from column 4 in Table 1. Geometrical grid with coefficient 1.07 with 80 (solid line, circles), 60 (dashed line, squares) and 40 (dotted line, triangles) grid points, respectively.

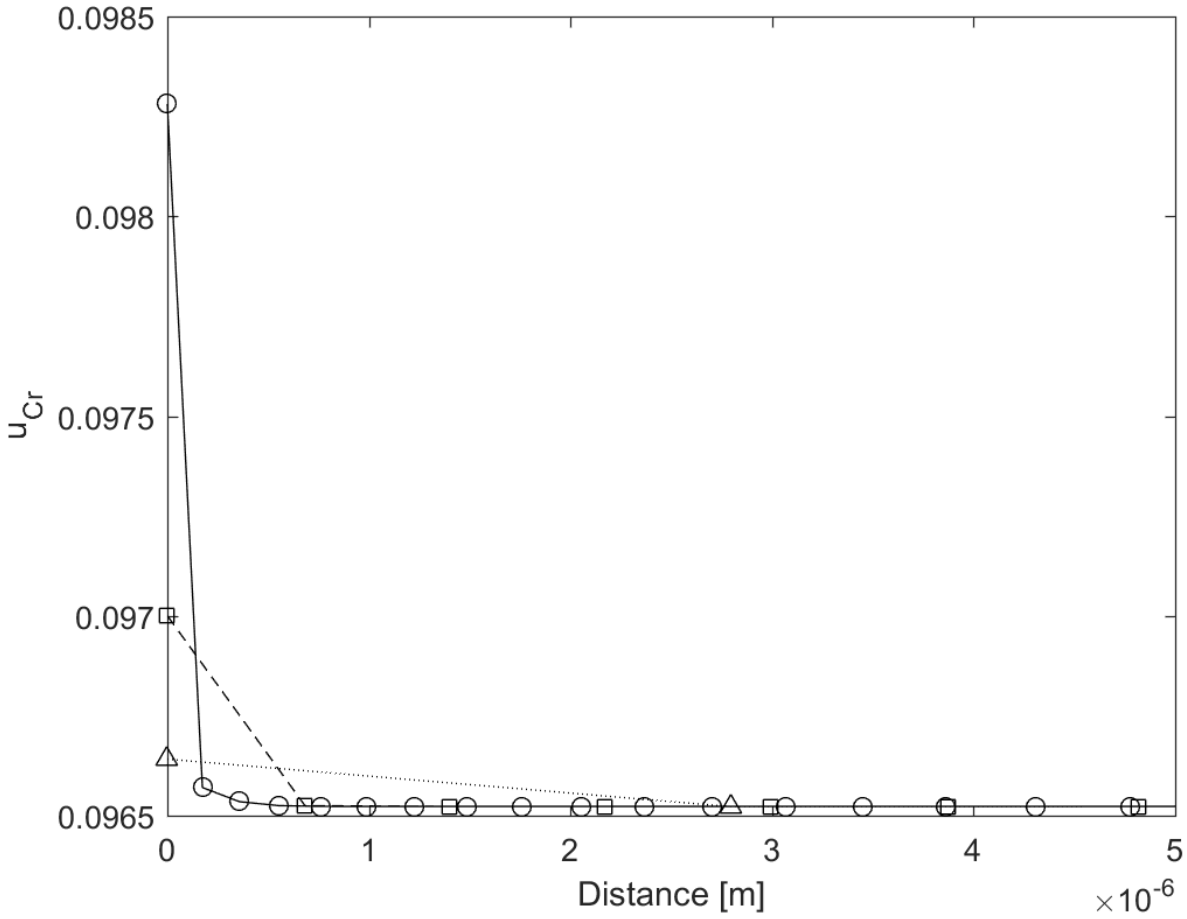

Figure 6: Comparison between results obtained at $t = 5.89 \cdot 10^7$ [s] with different grid point distributions. u-fraction chromium plotted as a function of distance. Close-up of surface region, cf. Figs. 4, 5, 7. Simulations performed at 600°C with interface reaction parameter taken from column 4 in Table 1. Geometrical grid with coefficient 1.07 with 80 (solid line, circles), 60 (dashed line, squares) and 40 (dotted line, triangles) grid points, respectively.

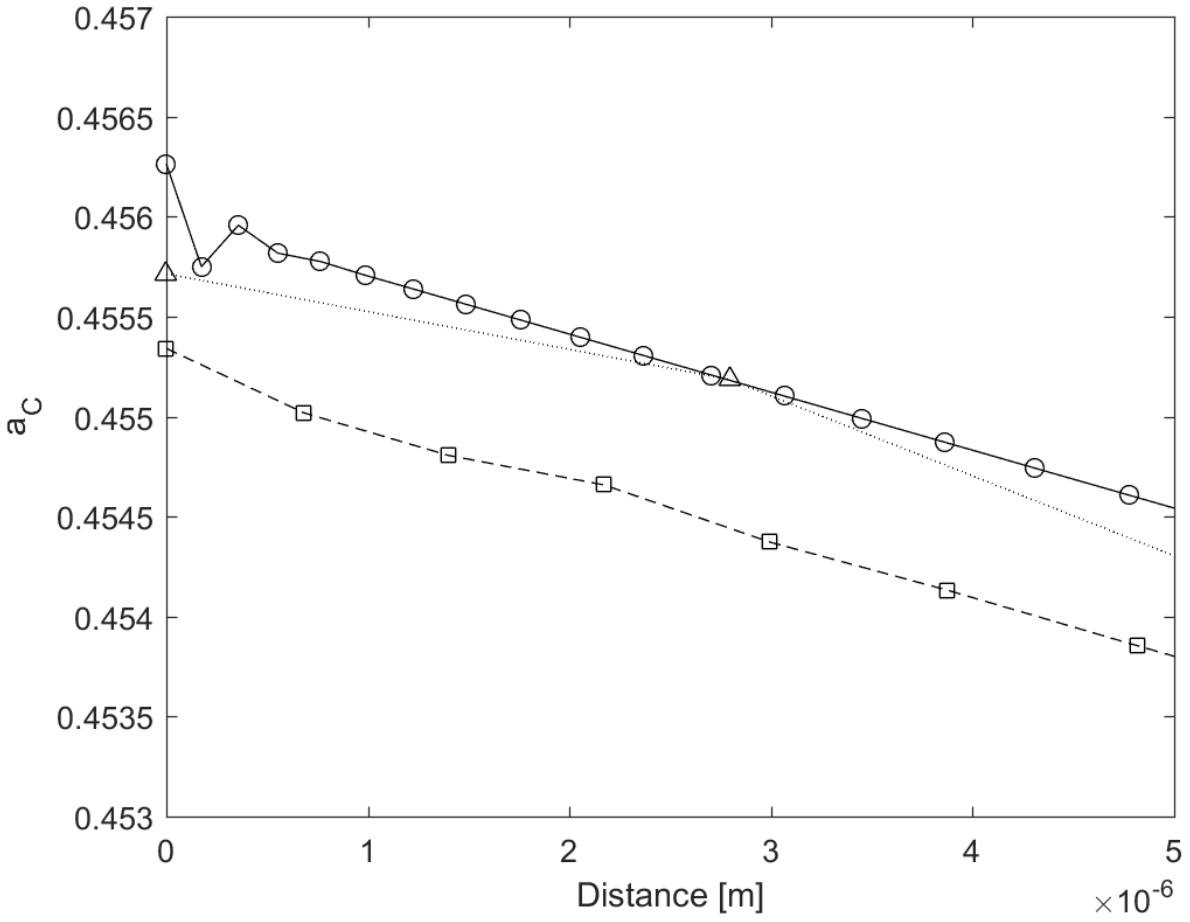

Figure 7: Comparison between results obtained at $t = 5.89 \cdot 10^7$ [s] with different grid point distributions. Carbon activity plotted as a function of distance. Close-up of surface region, cf. Figs. 4–6. Simulations performed at 600°C with interface reaction parameter taken from column 4 in Table 1. Geometrical grid with coefficient 1.07 with 80 (solid line, circles), 60 (dashed line, squares) and 40 (dotted line, triangles) grid points, respectively.

	t_{crit} [s]	
T[°C]	upper Hashin-Shtrikman bound	upper Wiener bound
520	6.69E+02	6.69E+02
600	1.64E+01	1.64E+01
640	3.33E+00	3.31E+00

Table 8: Time t_{crit} [kh] to reach $\eta_{\text{crit}} = 0.8$ for two different choices of homogenization functions. For these simulations the participating phases were $\alpha + M_7C_3 + M_{23}C_6 + M_6C$. The interface reaction parameter value used correspond to column c4 in Table 1.

	t_{crit} [kh]		
T [°C]	c1	c4	c8
400	8.27E+04	-	-
520	1.08E+02	6.62E+02	7.96E+03
600	3.38E+00	1.66E+01	1.19E+02
640	7.20E-01	3.47E+00	1.99E+01

Table 9: Time t_{crit} [kh] to reach a carbon content corresponding to $\eta_{\text{crit}} = 0.8$ at the surface under different conditions. For these simulations the participating phases were $\alpha + M_7C_3 + M_{23}C_6 + M_6C$. Diffusion of only carbon were included in the simulations, as conducted by the numerical model developed by Gong *et al.*

5.8 Effect of homogenization function

Three of the simulations of section 5.2 were repeated using the upper Hashin-Shtrikman bound instead of the upper Wiener bound. Results are shown in Table 8. It can be seen that the differences are negligible.

5.9 Effect of Jacobian perturbation parameter and a note on the degree of implicity

These settings do not affect results but may have an effect on simulation speed.

Simulations were run with the Jacobian perturbation parameter equal to 10^{-3}, 10^{-4} and 10^{-5} with no significant difference in simulation speed; as a rule-of-thumb difference smaller than 10% can be disregarded (or simulations must be repeated multiple times to obtain better statistics).

Homogenization model simulations should generally be run with fully implicit time-stepping (Euler backward) rather than semi-implicit (trapezoidal rule). Even though the trapezoidal rule is a higher order method compared to Euler backward and therefore may be expected to result in somewhat faster simulations an opposite, and more significant, the effect is more common. A test for the current work resulted in Euler backward being more than ten times faster than the trapezoidal rule.

5.10 Comparisons with numerical models developed by Gong *et al.*

Gong *et al.* developed numerical models to treat carbon uptake in the alloy substrate[2]. The underlying governing equations are in principle consistent with those implemented in DICTRA including the diffusion equation and the boundary conditions (activity flux function), though only carbon diffusion is taken into account in Gong's model (as justified in the main text of this paper). The major aim of Gong's treatment is to speed up simulations, which are useful for (1) fitting to measured carbon profiles and (2) extending to complex geometries of simulation domains. Table 9 lists predicted times t_{crit} [kh] to reach a carbon content corresponding to $\eta_{\text{crit}} = 0.8$ at the surface under conditions, as performed by using Gong's numerical models. One can see those values are within ±10% compared with Table 3.

6 Summary and discussion

The DiCTra work performed by Gong and Reed [2] is good and proper. General suggestions and guidelines for the usage of the homogenization model have been outlined. All simulation results performed during the course of the present review are available digitally upon request.

Since the diffusion of Fe, Cr and Mo may be disregarded, a simplified model that only allows for carbon diffusion, but which does allow for 2D simulations, should yield quantitatively correct results. Geometrical effects should be of practical importance.

Simulations that include both the oxide scale growth and the internal carburisation are currently not feasible. Even if they were it is doubtful if such simulations would be of practical use since the rate of carbon diffusion through the oxide scale still would be governed by what would amount to a fitting parameter; grain boundary diffusivity data is scarce and, to complicate matters further, some grain growth may occur. However, some refinements should be possible; a tailor-made boundary condition that allows metal loss into the oxide to be taken into account, but still contains a fudge factor to be of practical use, could possibly be implemented.

It would be of interest to simulate the evolution of the particle size distribution of the carbide phases. TC-PRISMA [30] (Thermo-Calc precipitation module) is a software tool for simulating the evolution of particle size distributions. However, in TC-PRISMA it is currently not possible to have non-closed boundary conditions, i.e. precipitation can only be driven by an initial supersaturation of a matrix phase.

References

[1] J-O Andersson, T Helander, L Höglund, P-F Shi, B Sundman, Calphad 26(2002)273.

[2] Y Gong, RC Reed, "Modelling of combined oxidation / carburisation of Fe-9Cr-1Mo-0.1C steel in CO_2", report NRS/CHEM/BEGL/P(18)228, Department of Materials & Department of Engineering Science, University of Oxford, 2018.

[3] Y Gong, DJ Young, P Kontis, YL Chiu, H Larsson, A Shin, JM Pearson, MP Moody, RC Reed, Acta Materialia 130(2017)361.

[4] H Larsson, A Engström, Acta Materialia 54(2006)2431.

[5] H Larsson, L Höglund, Calphad 33(2009)495.

[6] AE Stearn, H Eyring, J Phys Chem 44(1940)955.

[7] J Bardeen, Phys Rev 76(1949)1403.

[8] J Bardeen, C Herring, in: Atom Movements, ASM, Cleveland, Ohio, 1951, p. 87.

[9] JR Manning, Physical Review A 139(1965)A126.

[10] JR Manning, Metallurgical Transactions 1(1970)499.

[11] J-O Andersson, J Ågren, Journal of Applied Physics 72(1992)1350.

[12] H Larsson, T Jonsson, R Naraghi, Y Gong, RC Reed, J Ågren, Materials and Corrosion 68(2017)133.

[13] J Morral, BM Dupen, CC Law, Metallurgical Transactions A 23A(1992)2069.

[14] A Engström, L Höglund, J Ågren, Metallurgical and Materials Transactions A 25A(1994)1127.

[15] H Larsson, J Ågren, Metallurgical and Materials Transactions A 35A(2004)2799.

[16] O Wiener, Abhandlungen der Mathematisch-Physischen Klasse der Sächsischen Gesellschaft der Wissenschaften 32(1912)509.

[17] Z Hashin, S Shtrikman Journal of Applied Physics 33(1962)3125.

[18] Lord Rayleigh, Philosophical Magazine 34(1892)481.

[19] H Larsson, J Ågren, HTM Journal of heat treatment of materials 72(2017)1.

[20] K Bongartz, R Schulten, WJ Quadakkers, H Nickel, Corrosion 42(1986)390.

[21] N Matan, HMA Winand, P Carter, M Carutaratne, PD Bogdanoff, RC Reed, Acta Materialia 46(1998)4587.

[22] H Strandlund, H Larsson, Acta Materialia 52(2004)4695.

[23] L Sproge, J Ågren, Journal of Heat Treating 6(1988)9.

[24] G Dahlqvist, ÅBjörk, "Numerical Methods", Prentice-Hall, Englewood Cliffs, NJ, 1974.

[25] J Nocedahl, SJ Wright, "Numerical Optimization", Springer, New York, NY, 2006.

[26] HL Lukas, SG Fries, B Sundman, "Computational Thermodynamics — The Calphad Method", Cambridge University Press, Cambridge, UK, 2007.

[27] C Qiu, ISIJ International 32(1992)1117-1127.

[28] J Bratberg, Zeitschrift für Metallkunde 96(2005)335.

[29] B Jönsson, Zeitschrift für Metallkunde 85(1994)498.

[30] See `www.thermocalc.com`

[31] H Larsson and L Höglund, Calphad 50(2015)1.